Aalborg Universitet

AALBORG UNIVERSITY

Characterizations of Millimeter-Wave Reconfigurable Intelligent Surfaces in the Near-Field Region

Mei, Peng; Pedersen, Gert Frølund; Zhang, Shuai

Published in:
2023 Photonics and Electromagnetics Research Symposium, PIERS 2023 - Proceedings

DOI (link to publication from Publisher):
10.1109/PIERS59004.2023.10221249

Creative Commons License
CC BY 4.0

Publication date:
2023

Document Version
Accepted author manuscript, peer reviewed version

Link to publication from Aalborg University

Citation for published version (APA):
Mei, P., Pedersen, G. F., & Zhang, S. (2023). Characterizations of Millimeter-Wave Reconfigurable Intelligent Surfaces in the Near-Field Region. In *2023 Photonics and Electromagnetics Research Symposium, PIERS 2023 - Proceedings* (pp. 2079-2085). Article 10221249 IEEE (Institute of Electrical and Electronics Engineers). https://doi.org/10.1109/PIERS59004.2023.10221249

General rights
Copyright and moral rights for the publications made accessible in the public portal are retained by the authors and/or other copyright owners and it is a condition of accessing publications that users recognise and abide by the legal requirements associated with these rights.

- Users may download and print one copy of any publication from the public portal for the purpose of private study or research.
- You may not further distribute the material or use it for any profit-making activity or commercial gain
- You may freely distribute the URL identifying the publication in the public portal -

Take down policy
If you believe that this document breaches copyright please contact us at vbn@aub.aau.dk providing details, and we will remove access to the work immediately and investigate your claim.

Downloaded from vbn.aau.dk on: December 05, 2025

Characterizations of Millimeter-wave Reconfigurable Intelligent Surfaces in the Near-field Region

Peng Mei, Gert Frølund Pedersen, and Shuai Zhang
Antennas, Propagation and Millimeter-Wave Systems (APMS) Section
Department of Electronic Systems, Aalborg University, Aalborg, Denmark

Abstract— Reconfigurable intelligent surfaces (RISs) have been envisaged as a key and promising technology for evolved millimeter-wave 5G and upcoming 6G applications to enhance wireless communication channel capacity and quality. RISs are, in general, implemented with an electrically large size that is much larger than the wavelength at the frequency of interest. In some specific indoor application scenarios, such as intelligent factories, intelligent offices, intelligent shopping malls, etc., the users or targets are usually located at the near-field regions of the RISs. In these application scenarios, using RISs to perform near-field communications rather than conventional far-field communications might bring significant benefits. This paper will demonstrate our findings on the characterizations of millimeter-wave reconfigurable intelligent surfaces in the near-field regions, where it is found and concluded that using a near-field focusing RIS can indeed gain some benefits for wireless communications. Some figures of the metric of benefit distance and near-field gain are defined to quantitatively evaluate the benefits gained by the near-field focusing RIS. The findings will provide system-level reference and thumb of the rule of RISs for some indoor application scenarios, where the users are in the near-field region of the RIS.

1. INTRODUCTION

Reconfigurable intelligent surfaces (RISs) have emerged as a novel communication paradigm with tremendous potential for enhancing the performance of the evolved 5G and upcoming 6G wireless networks [1–4]. RISs are kinds of surfaces that are composed of lots of artificial elements, each of which can be controlled with electronic components such as PIN diodes or RF switches to manipulate the reflection phase of electromagnetic waves [5–9]. As a result, RISs have the capability to intelligently control the propagation of wireless signals, resulting in a significant reduction in interference at desired receivers and enhanced security against non-intended receivers, which can be achieved by manipulating the radiation beams of the RIS intelligently.

To date, most research related to RISs has focused on practical implementations based on far-field assumptions. Since a RIS is usually implemented with an electrically large aperture in terms of wavelength in the frequency of interest, in some scenarios where users or receivers are in the near-field region of a RIS, such as indoor applications, near-field assumptions should be adopted to evaluate its performance [10]. However, there is a lack of literature that systematically evaluates the electric-field activities in the near-field region of a RIS. A recent study examined the near-field behaviors of RISs using a simplified model, neglecting mutual couplings among elements and modeling radiation patterns as isotropic [11]. Despite the limitations, the study revealed the potential benefits of using RISs in near-field communications instead of conventional far-field communications. Near-field focusing, which can achieve a high-energy focal spot in the near-field region, is a critical technology in near-field wireless communications. The focal spot of a near-field focusing surface can be controlled by manipulating phases of radiating elements, making it a versatile tool for wireless power transfer [12, 13] and RFID reader applications [14–16].

This paper briefly summarizes some results of our previous work [17], where we conducted a comprehensive study and comparison of the characteristics of a RIS in its near-field region. The electric field is selected as the evaluation target, where the electric fields in the near-field region of both near-field focusing and conventional far-field RISs are simulated and compared. To quantify the performance of the near-field focusing RIS, we proposed and defined a metric called benefit distance, which represents the spatial distance that the near-field focusing RIS can outperform the conventional far-field RISs in terms of electric-field amplitudes. Within the benefit distance, the electric fields from the near-field focusing RIS are always stronger than the counterparts from the conventional far-field RIS. Another metric of near-field gain that is related to the position of the observation area is defined as the difference in electric fields between the near-field focusing and

conventional far-field RISs at the same positions. These metrics can provide a deeper understanding of the performance of RISs in near-field communication scenarios and can aid in the design of more efficient RIS-based communication systems.

2. APPLICATION SCENARIO

To demonstrate a potential use case for RISs in near-field communication scenarios, an application scenario is illustrated in Fig. 1. The RIS first receives the electromagnetic waves from the base stations and then directs them to users by manipulating the reflection phase of the RIS intelligently. It is well known that the electromagnetic field characteristics of an antenna vary as a function of distance, and as a result, the free space surrounding the antenna can be divided into two regions. The near-field region, which is closer to the antenna, is characterized by non-radiating electric and magnetic fields that dominate the behavior of the electromagnetic field. In contrast, the far-field region, which is further away from the antenna, is characterized by radiating fields that propagate through space.

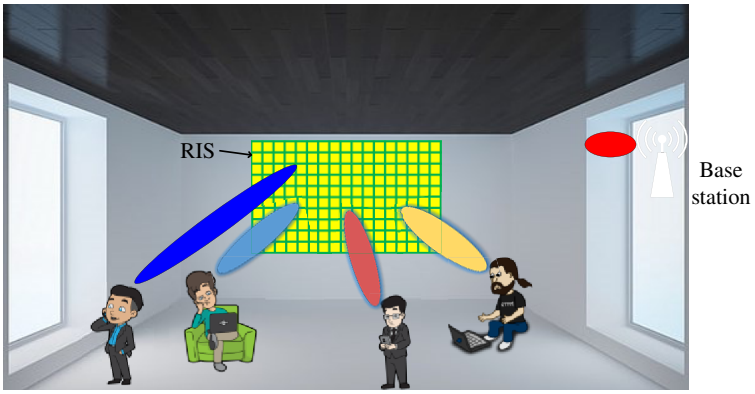

Figure 1: The diagram of application scenario of a near-field focusing RIS.

For a square-shaped aperture antenna, its near-field region is evaluated by [18]:

$$d = \frac{2D^2}{\lambda} \tag{1}$$

where D is the diagonal length (otherwise, it should be the largest dimension for an irregular-shaped aperture) of the aperture antenna. λ is the wavelength at the frequency of interest. Fig. 2 plots the near-field distance of a square-shaped RIS with varying sizes at 26 GHz using Eq. (1). As an example, a RIS with a dimension of 500 mm $\times$ 500 mm has a near-field distance of approximately 86.6 m. when the size of a RIS exceeds a few square meters, the near-field distance becomes significant, spanning several hundred meters and effectively covering the entire space of an indoor environment. This observation motivates the exploration of RISs for near-field wireless communication systems, as opposed to conventional far-field communications. In the following sections, we will discuss the characteristics of RISs in their near-field regions and the potential advantages of using RISs to perform near-field focusing for wireless communications.

3. PERFORMANCE ANALYSIS OF A RIS IN ITS NEAR-FIELD REGION

To describe the radiation beam of a conventional far-field RISs, it is often characterized by a solid angle (θ, φ) in the spherical coordinate. In contrast, a near-field focusing RIS has an additional degree of freedom, and the location of the focal spot can be controlled using (r, θ, φ) in the spherical coordinate. The additional degree of freedom allows for greater control over the position of the focal spot.

The manipulations of the focal spot of a near-field focusing RIS still rely on controlling the reflection phase of each element of the RIS. Fig. 3(a) presents a simple diagram of a RIS illuminated with an external source that can offer either spherical or plane wave, where the RIS usually consists of unit cells with a periodicity of around half-wavelength at the frequency of interest in free space. The RIS first receives the electromagnetic waves from the external source, after which it can achieve a focal spot at a position in the near-field region. For a focal spot at a specific position of (x_f, y_f, z_f),

the phase on element i of the RIS is formulated as:

$$\varphi(x_i, y_i, 0) = -\frac{2\pi}{\lambda}\left(\sqrt{(x_s - x_i)^2 + (y_s - y_i)^2 + (z_s)^2} + \sqrt{(x_f - x_i)^2 + (y_f - y_i)^2 + (z_f)^2}\right) \quad (2)$$

where (x_s, y_s, z_s) is the location of the phase center of the external source, $(x_i, y_i, 0)$ is the location of the element i in the RIS, and λ is the wavelength at the frequency of interest.

To investigate the performance and properties of a near-field focusing RIS, we constructed a 200 mm × 200 mm RIS using dielectric-based reflective elements with a periodicity of 5 mm, where the reflection phase of each element can be adjusted by tuning its height. We obliquely illuminated the RIS with a 10 dBi gain linearly-polarized horn antenna at 26 GHz, which generates a spherical wave. To ensure good aperture illumination and eliminate blockage effects, we set the location of the phase center of the horn antenna to (95 mm, 0, 106.5 mm), based on the radiation patterns of the horn antenna at 26 GHz. Using Eq. (2), we can calculate the phase distributions of elements on the RIS at 26 GHz with assigned focal distances of 80 mm, 200 mm, 300 mm, 400 mm, 500 mm, and 600 mm along the boresight direction (z-direction). The near-field focusing performance of the RISs is simulated with CST Microwave Studio software. An example of a simulation model established in CST is depicted in Fig. 3(b). Fig. 4(a) presents the electric fields in the z-direction from 0 to 1000 mm (corresponding to 0 to 87λ). It is observed that the simulated actual focal distance (the location of the peak electric-field amplitude) is smaller than the assigned value. The distance discrepancy between the locations of the actual and assigned focal spots is named focal shift, which is attributed to the field-spreading factor $1/R$ as explained in [19, 20]. The focal shift is increasingly remarkable with the increment of the assigned focal distance as seen in Fig. 4(a). Besides, the focal spot is becoming less concentrated with the increment of the assigned focal distance as observed from Fig. 4(a). Indeed, the electric-field distributions on the yoz-plane of the RISs with assigned focal distances of 80 mm and 300 mm are plotted and shown in Figs. 4(c) and (d), where the shape of the focal spot becomes longer for a larger focal distance.

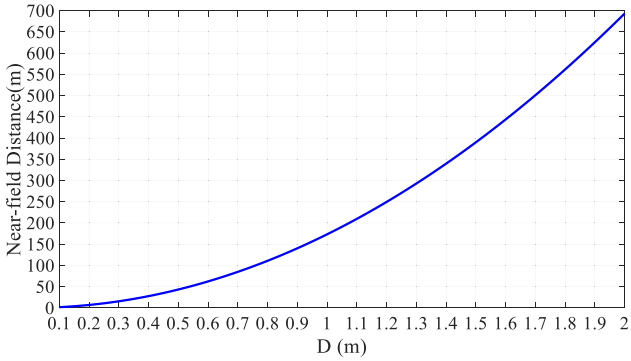

Figure 2: The calculated near-field distance with different aperture sizes at 26 GHz using Eq. (1). (D is the diagonal length of the square-shaped aperture).

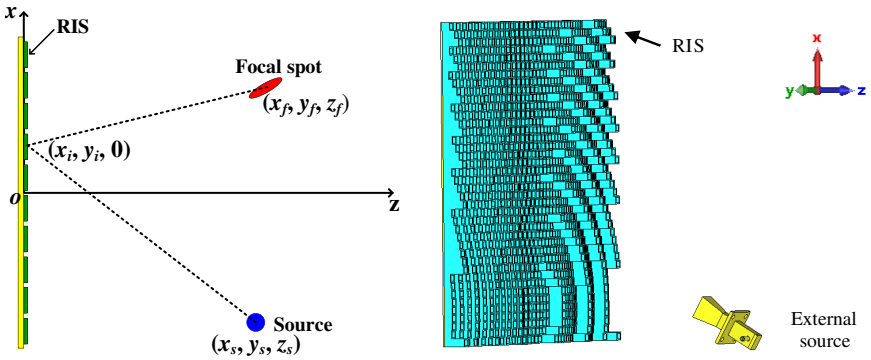

Figure 3: (a) A simple diagram of a RIS illuminated with an external source to achieve a focal spot in the near-field region. (b) An example of the simulation model in CST software.

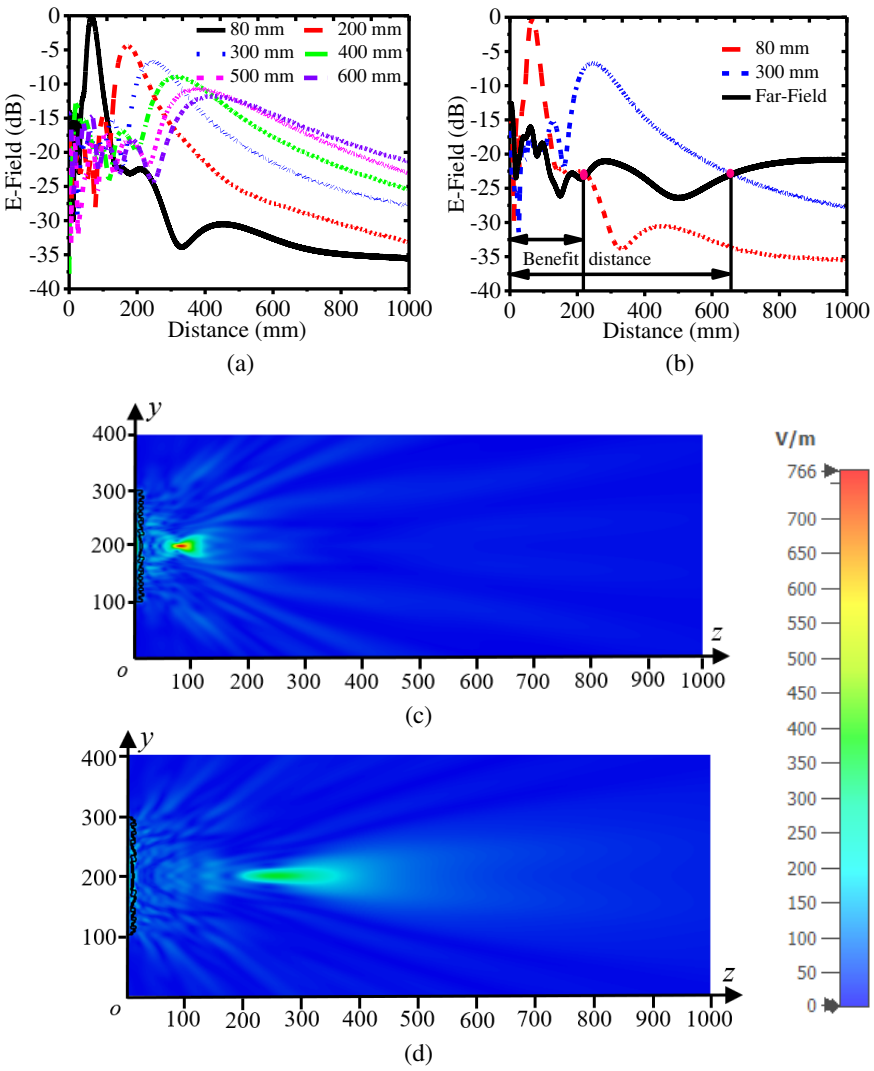

Figure 4: Near-field focusing performance of a RIS. (a) The electric field along the boresight direction with the assigned focal distances of 80, 200, 300, 400, 500, 600 mm. (b) The electric field along the boresight direction with the assigned focal distance of 80 and 300 mm, and the referred far-field. (c) The electric-field distribution on the *yoz*-plane with the assigned focal distance of 80 mm. (d) The electric-field distribution on the *yoz*-plane with the assigned focal distance of 300 mm. (The units for y- and z-axis are millimeters in both Figs. (c) and (d)).

To demonstrate the benefits of a RIS performing the near-field focusing, the electric fields of the conventional far-field RIS (RIS acts as a conventional directional reflector) along the boresight direction are also simulated. Fig. 4(b) reveals that the conventional far-field RIS does not possess a focal spot from 0 to 1000 mm, and there are points of intersection between the electric fields of the near-field focusing and far-field RISs. The longitude distance of the intersection point is defined as the benefit distance here. Within the benefit distance, the electric fields generated by the near-field focusing RIS are stronger than those of the conventional far-field RIS as seen in Fig. 4(b). Moreover, the benefit distance increases with the increment of the focal distance as observed in Fig. 4(b).

To assess the benefits that we can gain by using the near-field focusing RIS instead of the conventional far-field RIS, a cumulative distribution function (CDF) related to the electric-field enhancement is proposed and defined as:

$$F(x) = P((E_{focusing} - E_{ref}) \leq x) \tag{3}$$

where $E_{focusing}$ is the electric-field amplitude from the near-field focusing RIS at a specific location, and E_{ref} is the electric-field amplitude from the conventional far-field RIS at the same location. The difference between $E_{focusing}$ and E_{ref} is named near-field gain here (e.g., Near-field Gain

$= E_{focusing} - E_{ref}$). We use the decibels to describe the near-field gain in the following. When a near-field gain is positive, it means $E_{focusing}$ is stronger than E_{ref}. The CDF implies the probability of the near-field gain less than a certain value in the area of interest which can be a line, a plane, or a volume.

To accommodate scenarios involving mobile users effectively, it is crucial for the RISs to have the ability to steer its radiation beam or focal spot. By selecting the points with the highest powers from all scanning beams or focal spots within a 2- or 3-dimensional space, a total scan pattern can be formed in a plane or volume accordingly. For demonstration, we select an area of 400 mm × 400 mm on the *yoz*-plane as the region of interest to reduce the simulation time and eliminate the blockage effects of the external source (horn antenna). The total scan patterns from the near-field focusing and conventional far-field RISs have been simulated and plotted, where the CDFs related to the near-field gain are calculated then according to the total scan patterns.

Here, we investigate and calculate the CDFs of the near-field focusing RISs. Figs. 5(a) and (b) plot the total scan patterns of the near-field focusing RIS with assigned focal distances of 80 mm and 300 mm in the region of interest, respectively. The scan patterns reveal that the focal spots are scanned along the arcs of the assigned focal distances. Furthermore, the total scan pattern of the conventional far-field RIS at the same area of interest is also plotted in Fig. 5(c). As a result, the corresponding CDFs related to the electric field enhancement of the near-field focusing RISs with assigned focal distances of 80 mm and 300 mm compared to the conventional far-field RIS are calculated and shown in Fig. 6.

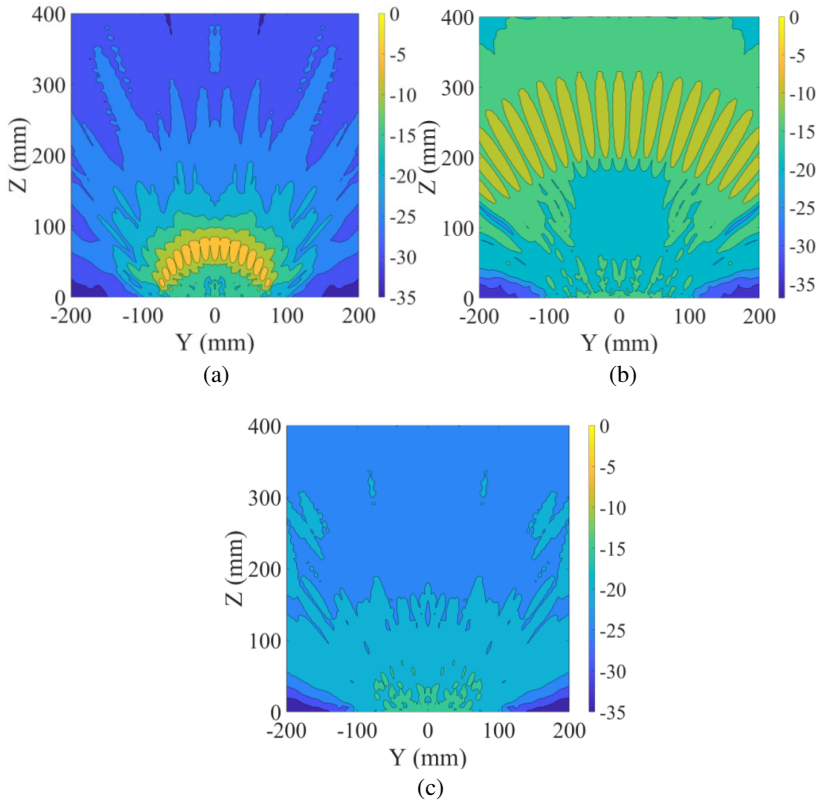

Figure 5: The total scan patterns within the area of interest (400 mm × 400 mm on the *yoz*-plane) at 26 GHz. (a) Near-field focusing RIS with an assigned focal distance of 80 mm. (b) Near-field focusing RIS with an assigned focal distance of 300 mm. (c) Conventional far-field focusing RIS. (All values are normalized to the maximum electric-field amplitude of Fig. 6(a).)

Note that the results in Fig. 6 have already included the conventional far-field RIS case as the near-field gain is defined as the difference between $E_{focusing}$ and E_{ref}. The maximum near-field gains are 15 dB and 17 dB for the near-field focusing RISs with assigned focal distances of 80 mm and 300 mm, respectively. On the other hand, the probability that the electric fields from a near-field focusing RIS stronger than those from the conventional far-field RIS in the area of interest with respect to a certain near-field gain value can be directly observed from the CDFs shown in

Fig. 6. For the near-field focusing RIS with an assigned focal distance of 80 mm, the value of the corresponding CDF is 0.78 when the near-field gain is 0 dB. The value of 0.78 means the region that electric fields from the near-field focusing RIS are stronger than those of the conventional far-field RIS accounts for 22% of the area of interest (400 mm × 400 mm). In contrast, the value of the CDF is only 0.09 when the near-field gain is 0 dB for the near-field focusing RIS with an assigned focal distance of 300 mm.

As seen in Fig. 6, the CDFs of the near-field focusing RISs with assigned focal distances of 80 mm and 300 mm are greatly distinct (the slopes of the curves are different). Specifically speaking, the probabilities differ noticeably when the near-field gain is 0 dB, they are 0.78 and 0.09. The differences of the CDFs can be explained by the 1-D electric fields shown in Fig. 4(b). Compared to the dimension of the area of interest (400 mm × 400 mm (*yoz* plane)), the electric fields from the near-field focusing RIS with an assigned focal distance of 300 mm are always stronger than those of the conventional far-field RIS within 400 mm as the benefit distance of the near-field focusing RIS is around 650 mm. In contrast, as the benefit distance with an assigned focal distance of 80 mm is only around 180 mm, the electric fields of the near-field focusing RIS are only stronger than those of the conventional far-field RIS within 180 mm. Beyond the benefit distance (from 180 to 400 mm), the electric fields of the near-field focusing RIS are weaker than those of the conventional far-field RIS.

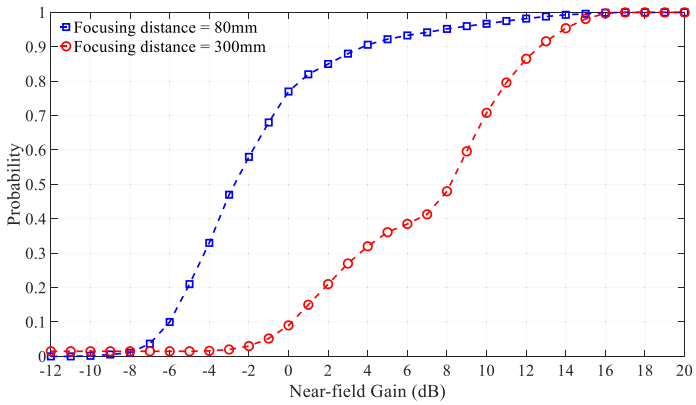

Figure 6: The calculated CDFs of near-field gain of near-field focusing RISs with assigned focal distances of 80 and 300 mm.

It should be mentioned here, the CDF is also affected by the size of the region of interest. Specifically speaking, for a near-field focusing RIS with an assigned focal distance of 300 mm, the CDFs will be different when the areas of interest are 400 mm × 400 mm and 600 mm × 600 mm. The maximum near-field gains might keep the same but the probability that the near-field gain is higher than an identical value will be distinct.

4. CONCLUSION

In this paper, we have conducted a comprehensive study of the near-field behaviors of a near-field focusing RIS. By comparing the electric fields from near-field focusing and conventional far-field RISs in the near-field region, we observed that the electric fields from the near-field focusing RIS are stronger than those from the conventional far-field RIS in certain regions. To evaluate the advantages of using near-field focusing RIS, we have defined metrics such as benefit distance, near-field gain, and cumulative distribution function (CDF) related to the electric-field enhancement.

Through our analysis of near-field focusing RISs with assigned focal distances of 80 mm and 300 mm, we have concluded that a larger focal distance leads to a larger benefit distance and a smaller near-field gain. Furthermore, the benefit distance has a direct impact on the CDF. Typically, a larger benefit distance results in a smaller probability in the area of interest as indicated by the CDF when the near-field gain is equal to a certain value.

In indoor wireless communication scenarios, if the entire room is within the near-field region of a RIS, using a RIS for near-field focusing can bring significant benefits compared to a conventional far-field RIS. By knowing the users' locations and the desired power they need to receive, we can assess the near-field gain based on the transmitted power from the base station. This information can help determine the optimal size of the RIS needed for effective near-field wireless communications.

REFERENCES

1. Basar, E., M. Di Renzo, J. De Rosny, M. Debbah, M. Alouini, and R. Zhang, "Wireless communications through reconfigurable intelligent surfaces," *IEEE Access*, Vol. 7, 116753–116773, 2019.
2. Huang, C., A. Zappone, G. Alexandropoulos, M. Debbah, and C. Yuen, "Reconfigurable intelligent surfaces for energy efficiency in wireless communication," *IEEE Trans. Wireless Commun.*, Vol. 18, No. 8, 4157–4170, Aug. 2019.
3. Basar, E. and I. Yildirim, "Reconfigurable intelligent surfaces for future wireless networks: A channel modeling perspective," *IEEE Wireless Commun.*, Vol. 28, No. 3, 108–114, Jun. 2021.
4. Yildirim, I., A. Uyrus, and E. Basar, "Modeling and analysis of reconfigurable intelligent surfaces for indoor and outdoor applications in future wireless networks," *IEEE Trans. Commun.*, Vol. 69, No. 2, 1290–1301, Feb. 2021.
5. Dai, L., et al., "Reconfigurable intelligent surface-based wireless communications: Antenna design, prototyping, and experimental results," *IEEE Access*, Vol. 8, 45913–45923, 2020.
6. Yang, H., F. Yang, S. Xu, Y. Mao, M. Li, X. Cao, and J. Gao, "A 1-bit 10×10 reconfigurable reflectarray antenna: design, optimization, and experiment," *IEEE Trans. Antenna Propag.*, Vol. 64, No. 6, 2246–2254, Jun. 2016.
7. Kamda, H., T. Iwasaki, J. Tsumochi, T. Kuki, and O. Hashimoto, "60-GHz electronically reconfigurable large reflectarray using single-bit phase shifters," *IEEE Trans. Antenna Propag.*, Vol. 59, No. 7, 2524–2531, Jul. 2011.
8. Carrasco, E., M. Barba, and J. A. Encinar, "X-band reflectarray antenna with switching-beam using PIN diodes and gathered elements," *IEEE Trans. Antenna Propag.*, Vol. 60, No. 12, 5700–5708, Dec. 2012.
9. Mei, P., S. Zhang, and G. F. Pedersen, "A low-cost, high-efficiency and full-metal reflectarray antenna with mechanically 2-D beam-steerable capabilities for 5G applications," *IEEE Trans. Antenna Propag.*, Vol. 68, No. 10, 6997–7006, Oct. 2020.
10. Di Renzo, M., A. Zappone, M. Debbah, M. Alouini, C. Yuen, J. Rosny, and S. Tretyakov, "Smart radio environments empowered by reconfigurable intelligent surfaces: How it works, state of research, and the road ahead," *IEEE J. Sel. Areas. Commun.*, Vol. 38, No. 11, 2450–2525, Nov. 2020.
11. Bjornson, E. and L. Sanguinetti, "Power scaling laws and near-field behaviors of massive MIMO and intelligent reflecting surfaces," *IEEE Open Journal of the Commun. Society*, Vol. 1, 1306–1324, 2020.
12. Yu, S., H. Liu, and L. Li, "Design of near-field focused metasurface for high-efficient wireless power transfer with multifocus characteristics," *IEEE Trans. Ind. Electron.*, Vol. 66, No. 5, 3993–4002, May 2019.
13. Zhang, P., L. Li, X. Zhang, H. Liu, and Y. Shi, "Design, measurement and analysis of near-field focusing reflective metasurface for dual-polarization and multi-focus wireless power transfer," *IEEE Access*, Vol. 7, 110387–110399, 2019.
14. Buffi, A., A. A. Serra, P. Nepa, H. T. Chou, and G. Manara, "A focused planar microstrip array for 2.4 GHz RFID readers," *IEEE Trans. Antenna Propag.*, Vol. 58, No. 5, 1536–1544, Mar. 2010.
15. Chou, H. T., M. Y. Lee, and C. T. Yu, "Subsystem of phased array antennas with adaptive beam steering in the near-field RFID applications," *IEEE Antennas Wireless Propag Lett.*, Vol. 14, 1746–1749, 2014.
16. Chou, H. T., T. M. Hung, N. N. Wang, C. Tung, and P. Nepa, "Design of a near-field focused reflectarray antenna for 2.4 GHz RFID reader applications," *IEEE Trans. Antenna Propag.*, Vol. 59, No. 3, 1013–1018, Mar. 2011.
17. Mei, P., Y. Cai, K. Zhao, Z. N. Ying, G. F. Pedersen, X. Q. Lin, and S. Zhang, "On the study of reconfigurable intelligent surfaces in the near-field region," *IEEE Trans. Antenna Propag.*, Vol. 70, No. 10, 8718–8728, Oct. 2020.
18. Balanis, C. A., *Antenna Theory: Analysis and Design*, 4th Edition, John Wiley & Sons. Inc., Hoboken, New Jersey, 2016.
19. Buffi, A., P. Nepa, and G. Manara, "Design criteria for near-field-focused planar arrays," *IEEE Antennas Propag Mag.*, Vol. 54, No. 1, 40–50, Feb. 2012.
20. Hansen, R. C., "Focal region characteristics of focused array antennas," *IEEE Trans. Antennas Propag.*, Vol. AP-33, No. 12, 1328–1337, Dec. 1985.